Superconducting Emitter Powered at 1.5 Terahertz by an External Resonator

Y. Ono,[1,*] H. Minami,[1,2,†] G. Kuwano,[1] T. Kashiwagi,[1,2] M. Tsujimoto,[1,2] K. Kadowaki,[3] and R. A. Klemm[4]

[1] *Graduate School of Pure and Applied Sciences, University of Tsukuba, 1-1-1 Tennodai, Tsukuba, Ibaraki 305-8573, Japan*

[2] *Division of Materials Science, University of Tsukuba, 1-1-1 Tennodai, Tsukuba, Ibaraki 305-8573, Japan*

[3] *Algae Biomass and Energy System (ABES) Research and Development Center, University of Tsukuba, 1-1-1 Tennodai, Tsukuba, Ibaraki 305-8572, Japan*

[4] *Department of Physics, University of Central Florida, 4111 Libra Drive, Orlando, Florida 32816-2385, USA*

(Received 11 December 2019; revised manuscript received 13 April 2020; accepted 6 May 2020; published 11 June 2020; corrected 14 July 2020)

A different type of terahertz emitter is made by coupling a source mesa fabricated from the intrinsic Josephson junctions present in single-crystalline high-T_c superconducting $Bi_2Sr_2CaCu_2O_{8+\delta}$ (Bi2212) to a much larger and impedance-matched external resonator with resonance frequencies up to 1.5 THz. The lateral dimensions of the source mesa are only 20×20 μm^2, about 0.5%–3% of those of conventional Bi2212 mesas, but its thickness of 2 μm is comparable to them. The observed emission frequencies that lie near to 1.5 THz match very well the resonance frequencies of the external resonator. This result ensures that the functions of resonator and antenna are separated from that of the THz current source in the Bi2212 mesa structure. These facts allow for much greater flexibility in the emitter design to achieve higher power and higher frequency THz wave sources.

DOI: 10.1103/PhysRevApplied.13.064026

I. INTRODUCTION

Terahertz (THz) electromagnetic waves in the frequency f range between 0.1 and 10 THz have recently attracted much attention because of their enormous potential applications to various fields such as nondestructive imaging, spectroscopy, astronomy, medical sciences, food industries, high-speed communications, etc. [1,2]. For such versatile applications, compact, high-performance, all-solid-state, and continuous-wave (cw) monochromatic THz sources are inevitably demanded. Resonant tunneling diodes (RTDs) operating at room temperature [3–5] and quantum cascade lasers (QCLs) [6,7] may be good candidates. The emission power P of RTDs above the central frequency of the THz gap around 1.5 THz at present, however, is severely limited to about 1 μW [8]. It falls off exponentially with increasing f above 1 THz [9,10]. The emission power of QCLs below the operating maximum temperature T_{max} (K) $= (h/k_B)f \approx 50f$ (THz), where h and k_B are Planck's and Boltzmann's constants, falls off exponentially with decreasing f below 2.5 THz [6]. So far, the maximum cw power is reported to be 0.36 mW at 10 K and 40 μW at 58 K at 1.34–1.58 THz [11]. For frequencies near to 1 THz, the difference-frequency generation QCL (DFG-QCL) technique appears to be very promising at room temperature [12], but the recent reported power of DFG-QCL is still limited to only 20 μW below 2 THz at 78 K [13]. Thus, source frequencies around 1.5 THz are the most difficult to obtain and have been avoided as a "death valley" in spectroscopy. Here, we describe a different kind of device that is designed to overcome those difficulties.

In 2007, cw THz emission was discovered from single-crystalline high-T_c superconductor $Bi_2Sr_2CaCu_2O_{8+\delta}$ (Bi2212) mesa structures [14]. This compound consists of a regular c-axis array of superconducting CuO_2 double layers separated by insulating Bi_2O_2 layers, forming a stack of *intrinsic Josephson junctions* (IJJs) [15]. When a typical rectangular mesa structure with dimensions of $60 \times 300 \times 2.0$ μm^3 is biased by a dc voltage V across its IJJs, THz electromagnetic waves are generated according to the ac Josephson relation [16]: $f = (2e/h)(V/N)$, where N is the number of IJJs, e is the elementary charge, and $2e/h = 0.483\,597\,848\,4 \cdots$ THz/mV. In order to have strong coherent THz emission, nearly all of the IJJs must synchronize. In previously reported Bi2212 devices, P was enhanced by the cavity resonance effect of the mesa structure [14,17]. Impedance matching at the surface of the mesa to the external medium [18], heat removal, and hot-spot management are also important for high f and high P [19–23]. The advantage of the IJJ emitter over RTDs and QCLs lies in its continuous f tunability with V, allowing one to widely span 1.5 THz [24,25]. Recently, broadly

*onoyukino080227@gmail.com
†minami@bk.tsukuba.ac.jp

tunable THz wave emission was indeed reported between 1 and 11 THz from on-chip devices of both IJJ emitter and detector [26]. To date, the emission power P from a single IJJ mesa structure was estimated to be a few tens of microwatts at sub-THz frequencies [17,27–29]. A three-mesa array was reported to emit with $P \sim 0.61$ mW at 0.51 THz [30], but it appears that Joule heating hinders the coherent coupling of more than four mesa arrays.

In those previously reported mesa devices, the mesa itself works as an internal resonator [14,17,19,21–33]. Assuming its fundamental TM(1,0) mode is enhanced, the width w of the mesa is equal to $\lambda/2n$, as pictured in Fig. 1(a), where λ is the wavelength of the emitted THz wave in vacuum and n is the refractive index of Bi2212, which is about 4.2. To attain 1 THz with the TM(1,0) mode or higher-f radiation from that device structure, w of the rectangular mesa would be 36 μm. Therefore, the fabrication process of such Bi2212 mesa structures has to be precise, with width variations of less than approximately 1 μm [31,34]. This may have been the primary reason why it was previously difficult to realize higher-frequency emitters, especially above 1 THz. To overcome this problem, the higher-order resonance modes of relatively large mesas were intentionally used. As a result, THz emission was obtained over the wide frequency range of 0.3–2.4 THz, where powers of approximately 1 μW at 1 THz and of approximately 0.1 μW at 1.6 THz were found [24,25].

Here, we demonstrate an entirely different type of emitter using Bi2212 as the source but not as the resonator to generate coherent emissions above 1 THz. The design of the emitter has been greatly modified, as shown in Fig. 1.

In Fig. 1(a), the sketched conventional Bi2212 mesa structure simultaneously functions both as the THz current source and as the resonance antenna. Here, it is emphasized that a paradigm shift is introduced to separate the functions of the resonator and the antenna from a single mesa structure. Therefore, the Bi2212 superconducting mesa works only as the THz current source, whose frequency can be controlled solely by the ac Josephson effect. The fabrication process of this IJJ emitter is much simpler than in previous devices, because the great care needed to produce the strictly controlled shape and dimensions is no longer necessary.

Although the optimal mesa height is conventionally about 2 μm to minimize the overheating effect and to maximize the emission power, the lateral dimensions of the mesas can be much smaller, about 0.5%–3% of that of the previous mesas. The external resonator is arranged independently by assembling a parallel Au plate, as pictured in the right-hand panel of Fig. 1(a) and in Fig. 1(b). In the present device, the small Bi2212 source mesa is placed between a thin square Au plate resonator and a larger Bi2212 base plate.

This idea was proposed by previous computer simulation studies that indicated that the radiation efficiency

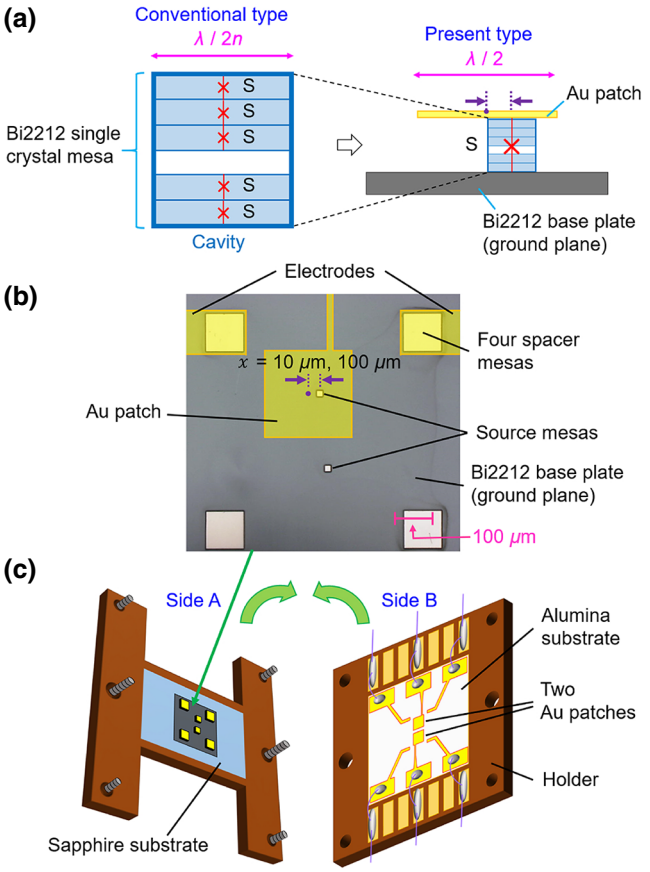

FIG. 1. Design of the THz emitter. (a) Paradigm shift of the device construction from the previous mesa source cavity-mode self-resonator (left) to the present mesa source external resonator (right). (b) A photograph of two source mesas and four spacer mesas fabricated on a single-crystalline Bi2212 surface with sketches of an external square Au patch resonator with electrodes. (c) Three-dimensional device overview.

could be improved over that of conventional mesas by using a small source mesa buried inside a dielectric medium and coupling it to an external patch antenna [35]. Based upon this idea, we build a prototype of such a THz emitter, and conduct performance test operations as described in detail in the following.

II. DEVICE FABRICATION

A high-quality Bi2212 single crystal is grown by the floating zone method. A piece of it is cut into thin square plates with lateral size of 1×1 mm^2 and a few tens of micrometers thick. The bottom of the device, Side A, sketched in the left-hand panel of Fig. 1(c), is first made by tightly gluing such a Bi2212 plate onto a sapphire substrate using polyimide resin. Then, just after cleaving the top surface of the Bi2212 plate down to a thickness of several micrometers, 10 nm of Ag and then of Au are deposited on its fresh surface. Next, using photolithography and Ar ion

milling techniques, two Bi2212 source mesas of dimensions $20 \times 20 \times 2.0\ \mu m^3$ and four Bi2212 electrode spacer mesas of dimensions $100 \times 100 \times 2.0\ \mu m^3$ are fabricated, as shown in Fig. 1(b). The top surface of the device, Side B, as sketched in the right-hand panel of Fig. 1(c), is first produced by a uniformly sputtered Au film, 0.5 μm thick, onto an alumina substrate. The Au film is then patterned by photolithography and Ar ion milling techniques into two patches and four current leads, eventually to be contacted to the two source mesas and to the four counter/spacer mesas, respectively. The sapphire (Side A) and the alumina (Side B) substrates are placed together face to face using sets of guide lines patterned on both substrates, and gently tightened by four screws at the corners of the copper holders, as shown in Fig. 1(c). To obtain reliable electrical contacts between the mesas and the patches/electrodes, the resistance of the device is monitored during the tightening of the screws. THz radiation is observed through the top alumina substrate, whose transmittance is 55%–65% at 0.5–1.5 THz.

Device A consists of a Bi2212 source mesa and of a thin Au patch antenna with lateral dimensions of $300 \times 300\ \mu m^2$. The resonance frequency is designed to be 0.5 THz so as to match the lowest TM(1,0) mode frequency. On the Au patch, the Bi2212 source mesa is placed about $x = 10\ \mu$m away from its center [see Fig. 1(b)]. After all the properties of Device A are measured, Device B is again constructed by opening the emitter and moving the source mesa to the position of $x = 100\ \mu$m away from the center of the Au patch. These mesa positions relative to the center of the Au patch are sketched in Fig. 1(b). For Device C, another source mesa is fixed onto a thin Au patch of dimensions $150 \times 150\ \mu m^2$, and its resonance frequency is designed to be 1.0 THz corresponding to its TM(1,0) mode. The Bi2212 source mesa is placed closer to an edge of the resonator, as in Device B.

Figure 2 shows the temperature dependencies of the c-axis resistance (R-T curves) for Devices A, B, and C measured by a two-terminal method. The superconducting transition temperature T_c is 81 K for Devices A and B and 85 K for Device C. Judging from these values as well as from the degree of increase in R with the decrease in T just above T_c, the Bi2212 crystals in Devices A and B may be slightly underdoped, while Device C (with the highest T_c) may be closer to optimal doping. The normal state resistances for these mesas are much larger than those for previous mesa devices, simply because the areal sizes of the present mesas are much smaller than those of the previous mesas. Note that the R-T curve of Device B is measured after the measurements for Device A. This reconstruction of the emitting device directly indicates the reliability and the reproducibility of the device.

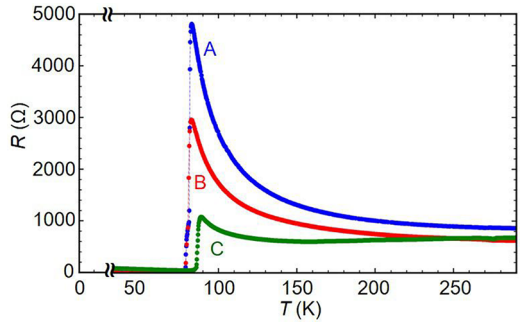

FIG. 2. The c-axis R-T curves of Devices A, B, and C.

III. MEASUREMENT SYSTEM

The device under study is mounted onto a cold finger of a ^{4}He flow cryostat (Oxford Instruments, CF1104). Figure 3(a) shows an overall schematic view of the THz measurement system used either for simple simultaneous THz detection and current-voltage characteristics (IVCs) measurements or for emission directivity measurements. The IVCs are measured by a conventional two-terminal method. For the detection of the THz radiation, a lock-in technique is used with an InSb hot-electron bolometer (HEB) detector (QMC Instruments, QFI/2BI) and a preamplifier with a gain of $\times 1000$ at a modulation frequency of 90 Hz by an optical chopper. Since the same setup is used as in previous experiments, direct comparisons with previous data can be made [27]. The optical sensitivity

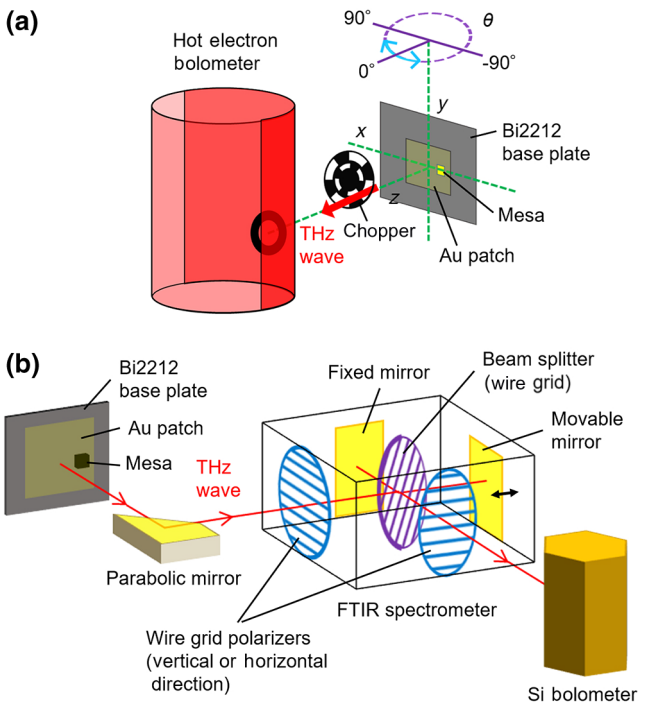

FIG. 3. Schematic view of the experimental setup (a) for radiation directivity measurements and (b) for frequency spectra and polarization measurements.

of the HEB is calibrated to be about 1.2 mV_{rms}/nW at around 0.5 THz, 0.6 mV_{rms}/nW at around 1.3 THz, and 0.30 mV_{rms}/nW at around 1.5 THz. The THz radiation is detected with an operating solid angle of 0.02 sr. Each point in the radiation pattern data is obtained from the THz intensities observed by tilting the device right and left every 5° to the HEB. The angle is defined to be 0° when the HEB is vertically above the Au patch. The sign of the rotation angle θ is defined to be positive when the device is rotated clockwise (top view) and negative when it is rotated counterclockwise.

The frequency spectra are measured using the system sketched in Fig. 3(b). The THz wave beam emitted from the IJJ THz emitter device is converted to a parallel beam by a concave mirror. Then it is guided to a Martin-Pupplet type of Fourier-transform infrared (FTIR) spectrometer (JASCO, FARIS-1) and the signal detected by a Si-composite bolometer (Infrared Laboratories, HDL-5) detector. This FTIR spectrometer has an experimental resolution limit of 8.0 GHz. The polarization characteristics are also measured by rotating the wire grid polarizers both at the entrance and exit of the FTIR interferometer to either the horizontal or vertical directions.

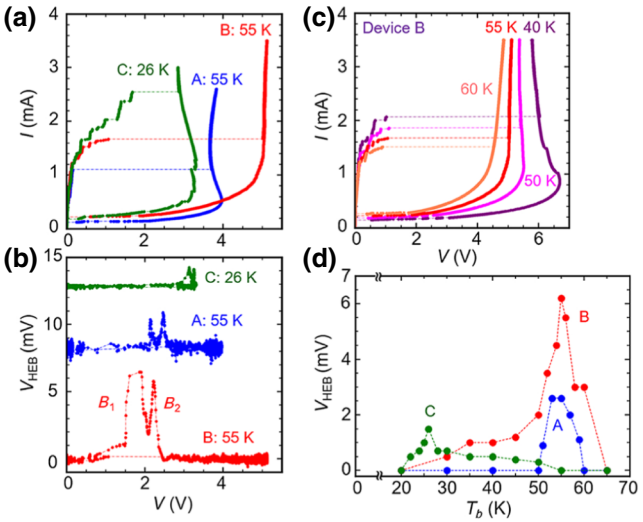

FIG. 4. Characteristics of Devices A, B, and C. (a) IVCs and (b) the corresponding HEB detector outputs for Devices A, B, and C. The data from Devices A and C are offset for clarity. (c) The set of IVCs at various T values from 40 to 60 K of Device B. (d) The base temperature T_b dependencies of the HEB detector outputs for Devices A, B, and C.

IV. RESULTS AND DISCUSSION

In Fig. 4(a), the IVCs obtained from Devices A and B at 55 K and from Device C at 26 K are displayed. Figure 4(b) shows the THz emission intensities simultaneously detected by the HEB while the IVC data shown in Fig. 4(a) are obtained. At these temperatures the THz emission intensities are the largest, as seen in Fig. 4(d). Considering the optical sensitivity of the HEB at each radiation frequency, the detected maximum power of Devices A, B, and C is 2, 5.2, and 2.5 nW, respectively.

In Fig. 4(c), a set of IVCs of Device B obtained between 40 and 60 K are shown. Device B shows excellent IVCs and radiation intensity behavior even after its reinstallation from Device A. For example, voltages larger than 6.5 V can be applied at 40 K without resulting in significant back-bending behavior indicative of suppressed overheating. These facts appear to indicate that good heat exhaustion conditions are met, which directly corresponds to the expected higher radiation frequency of about 2.3 THz at 40 K and potential to emit at around 1.5 THz at 60 K, as long as all the other conditions for the emission are satisfied.

In Fig. 5, we demonstrate that the Au patch antenna plays the major role for the determination of the THz radiation frequency. One of the most important conditions to be satisfied for THz emission is that the resonant frequency of the patch antenna must be equal to the ac Josephson frequency f_J. For the 300 × 300-μm^2 patch of Devices A and B and the 150 × 150-μm^2 patch of Device C, the fundamental resonance frequencies are designed to be 0.5 and 1.0 THz, respectively, which correspond to the infinitely degenerate TM(1,0) mode [36]. This is indeed seen in the 0.540 THz emission from Device A, as displayed in Fig. 5(a). Note that if the THz emission from the Bi2212 source mesa were to have been enhanced by one of its cavity resonances, the frequency of its lowest TM(1,0) mode for its lateral dimensions of 20 × 20 μm^2 would be about 1.79 THz. Therefore the Bi2212 emission could not have been enhanced by one of its cavity resonances, but the emission f is just determined by the ac Josephson effect, and the overall device P is enhanced by the TM(1,0) resonance of the Au patch antenna.

Figure 5(c) shows the angular THz radiation distribution pattern for Device A. It is highly directional and clearly different from the radiation pattern obtained from previously reported mesa devices [27,32,33]. From the results obtained from the present devices, the simultaneous dual source and resonator roles of previous device mesas are greatly modified. In the present devices, the Bi2212 mesa only has the role of the THz current source, whereas the Au patch antenna has the role of the external resonator. If this radiation pattern were also applicable to Device C, its integral power would be expected to be about 18 nW at 1.5 THz. Since the volume of the Bi2212 mesa of Device C is much smaller than that of the previously reported mesas, its radiation power P normalized by the mesa volume is estimated to be 4 times larger than that of a previous one emitting at almost the same frequency [24]. This result suggests that the output power P from previous large-area

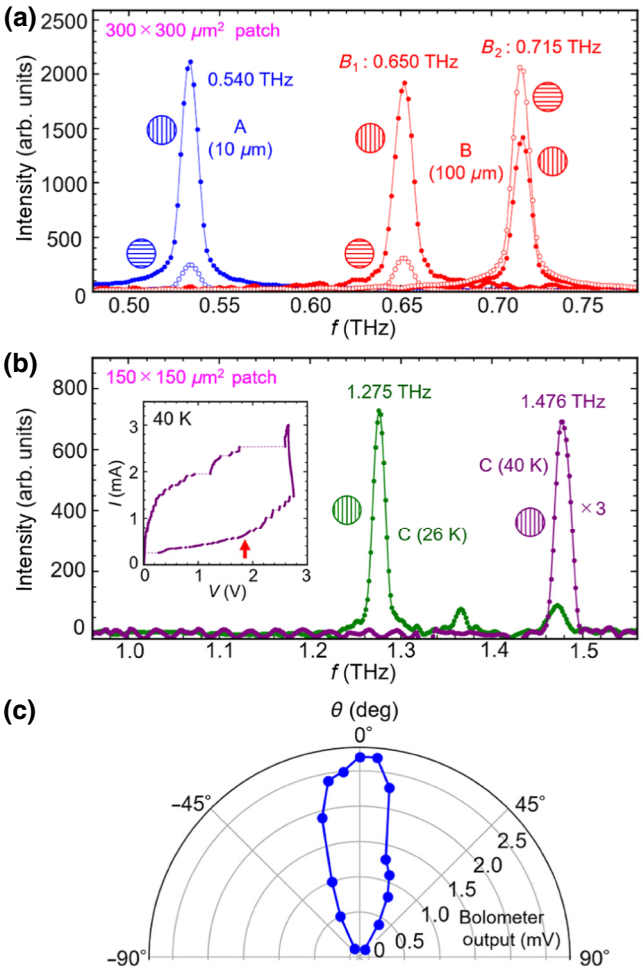

FIG. 5. Emission characteristics. (a) Observed THz emission spectra for Device A (blue) and Device B (red) at 55 K. (b) Observed THz emission spectra for Device C at 26 K (green) and 40 K (purple). Inset shows the I-V curve at 40 K and the arrow indicates the position where THz emission is observed. (c) Observed radiation pattern (directivity) for Device A.

mesa devices might have been limited from the optimal value, possibly by a lack of full IJJ synchronization.

Comparing the emission spectrum of Device B with that of Device A, it is noted that the emission frequency of 0.650 THz observed from Device B, corresponding to the emission peak labeled B_1 in Fig. 4(b), is up-shifted by about 18% from that of 0.540 THz observed from Device A. Furthermore, another emission from Device B is observed at 0.715 THz, as seen in Fig. 5(a), which is labeled B_2 in Fig. 4(b). This latter emission could arise from the excitation of the nondegenerate TM(1,1) mode of the Au patch antenna, which would be expected to be at 0.707 THz.

It is remarkable that Device C emits waves of around 1.5 THz at 40 K attained with a small cryo-cooler, as seen in Fig. 5(b). Note that the radiation frequencies of 1.275 and 1.476 THz observed from Device C at 26 and 40 K, respectively, are about twice those of the two frequencies observed from Device B, and they agree well with the results expected from the 150 × 150-μm^2 Au patch antenna, each side of which is half of that in Device B. As seen in the inset of Fig. 5(b), Device C emits in the low-current retrapping region at 40 K, where the number of Josephson junctions in the inactive (zero) voltage state is high. Compared to the radiation at 26 K in Fig. 4(b), the applied voltage to the entire mesa is lower, but it emits higher-frequency radiation at 40 K because the applied voltage per active junction is higher. Note that the linewidths of the spectra shown in Figs. 5(a) and 5(b) are not intrinsic, but are primarily determined by the experimental resolution of 8.0 GHz of the FTIR spectrometer. It is noted that the emissions at 1.476 THz are not far from the 1.414 THz expected for the excitation of the nondegenerate TM (1,1) mode of the Au patch of Device C [36].

V. SIMULATIONS

The actual observed THz modes are simulated with COMSOL software, using a realistic model in which a Bi2212 mesa of dimensions $20 \times 20 \times 2.0$ μm^3 is assumed to be placed on the wide surface of a Bi2212 single crystal of $1000 \times 1000 \times 10$ μm^3. A Au patch antenna of $300 \times 300 \times 2.0$ μm^3 with $\sigma = 4.9 \times 10^7$ S/m is assumed to be attached onto the top surface of the Bi2212 mesa. The relative permittivity is assumed to be $\epsilon_r \simeq 17$ for Bi2212, and the electric dc conductivity of $\sigma_a = \sigma_b = 1.0 \times 10^8$ S/m and $\sigma_c = 0.2$ S/m for the mesa, while $\sigma_a = \sigma_b = \sigma_c = 1.0 \times 10^8$ S/m for the Bi2212 base plate. The impedance of the mesa is set to be 10 Ω for THz current. Three excitation ports are placed on the two side surfaces and at the middle of the mesa. A rf in-phase voltage of 1 V is applied to the ports in the direction of the height.

Figures 6(a) and 6(c) show the computer-simulated radiation distribution patterns near the calculated resonance frequencies around 0.49 THz for Device A and around 0.585 THz for Device B, which are shifted downwards about 10% from the experimentally observed spectral lines A and B_1 in Fig. 5(a). These downshifted frequencies may be within the allowance due to the perturbation effect of the superconducting mesa on the resonator. On the other hand, the simulated pattern in Fig. 6(a) agrees pretty well with the observed one as shown in Fig. 5(c). Figures 6(b) and 6(d) show the electric field distributions during resonance for Devices A and B, respectively. As is clearly seen, the excited modes can be assigned to the TM(1,0) mode for output curve A of Device A shown in Fig. 5(a), whereas the TM(1,0) mode does not apply to output curve B_1 of Device B as shown in Fig. 5(a). This is perhaps because the low-impedance source mesa is attached far from the center of the resonator, resulting in the strongly deformed infinitely

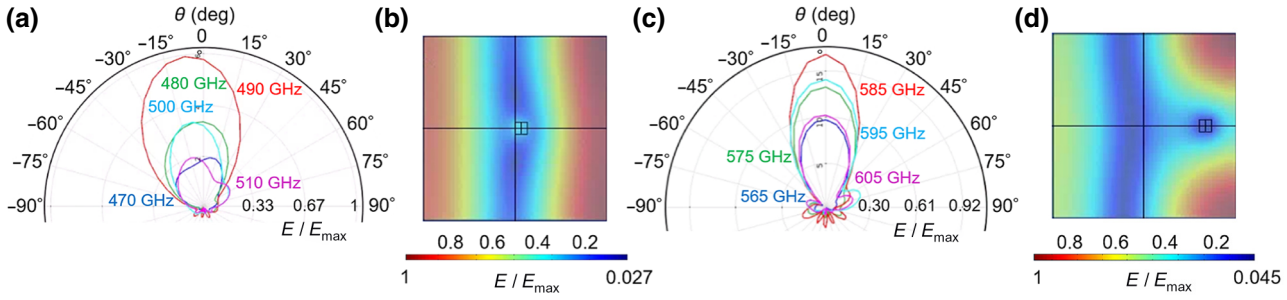

FIG. 6. The COMSOL simulation results. (a) Directivity and (b) electric field distribution for Device A. (c) Directivity and (d) electric field distribution for Device B.

degenerate TM(1,0) mode pattern [36]. This postulation can be tested by measuring the emission polarization with wire grids inserted along either the vertical (filled symbols) or the horizontal (open symbols) directions, as seen in Fig. 5(a). The spectral lines A and B_1 are found to be much stronger for the vertical polarization direction than for the horizontal one. On the other hand, the observed intensities of the differently polarized spectral lines B_2 shown in Fig. 5(a) are not very different, suggesting the polarization direction is tilted about 45° from the horizontal one. Somehow, this mode could not be reproduced in our simulations. As for the spectral line C observed for Device C and shown in Fig. 5(b), a large frequency upshift from the expected 1 THz is observed for the TM(1,0) Au patch antenna mode, but is close to 1.414 THz expected for the TM(1,1) Au patch antenna mode [36]. The behavior is similar to that observed for Device B, which could be related to the fact that both source mesas are located far away from the center of the Au patch, and could account for the excitations of the first excited state of the Au patch antenna.

VI. CONCLUSIONS

We demonstrate the feasibility of a particular IJJ THz emitter design, in which the roles of THz current source and resonator are separately assigned to the IJJs in a superconducting Bi2212 mesa and external Au patch antenna. This is achieved by coupling the external resonator to the IJJ emitter so as to synchronize the Josephson supercurrents generated in the IJJ mesa structure at a frequency of about 1.5 THz, in the central region of the remaining "THz gap" that has been the most difficult to fill using compact solid-state devices. This paradigm conceptual design change leads us to more practical IJJ emitters with much more flexibility and versatility for applications, which are much more reliable to fabricate reproducibly.

ACKNOWLEDGMENTS

This work is supported by JSPS KAKENHI Grants No. 15K04688 and No. 15H01996, and University of Tsukuba Basic Research Support Program Type B.

[1] M. Tonouchi, Cutting-edge terahertz technology, Nat. Photonics **1**, 97 (2007).
[2] S. S. Dhillon *et al.*, The 2017 terahertz science and technology roadmap, J. Phys. D: Appl. Phys. **50**, 043001 (2017).
[3] M. Asada and S. Suzuki, Room-temperature oscillation of resonant tunneling diodes close to 2 THz and their functions for various applications, J. Infrared Milli. Terahz. Waves **37**, 1185 (2016).
[4] S. Suzuki, M. Shiraishi, H. Shibayama, and M. Asada, High-power operation of terahertz oscillators with resonant tunneling diodes using impedance-matched antennas and array configuration, IEEE J. Sel. Top. Quantum Electron. **19**, 8500108 (2013).
[5] M. Feiginov, Frequency limitations of resonant-tunnelling diodes in sub-THz and THz oscillators and detectors, J. Infrared Milli. Terahz. Waves **40**, 365 (2019).
[6] B. S. Williams, Terahertz quantum-cascade lasers, Nat. Photonics **1**, 517 (2007).
[7] B. S. Williams, S. Kumar, Q. Hu, and J. L. Reno, High-power terahertz quantum-cascade lasers, Electron. Lett. **42**, 89 (2006).
[8] H. Kanaya, R. Sogabe, T. Maekawa, S. Suzuki, and M. Asada, Fundamental oscillation up to 1.42 THz in resonant tunneling diodes by optimized collector spacer thickness, J. Infrared Milli. Terahz. Waves **35**, 425 (2014).
[9] S. Suzuki, M. Asada, A. Teranishi, H. Sugiyama, and H. Yokoyama, Fundamental oscillation of resonant tunneling diodes above 1 THz at room temperature, Appl. Phys. Lett. **97**, 242102 (2010).
[10] T. Maekawa, H. Kanaya, S. Suzuki, and M. Asada, Oscillation up to 1.92 THz in resonant tunneling diode by reduced conduction loss, Appl. Phys. Express **9**, 024101 (2016).
[11] C. Walther, M. Fischer, G. Scalari, R. Terazzi, N. Hoyler, and J. Faist, Quantum cascade lasers operating from 1.2 to 1.6 THz, Appl. Phys. Lett. **91**, 131122 (2007).
[12] M. A. Belkin, F. Capasso, A. Belyanin, D. L. Sivco, A. Y. Cho, D. C. Oakley, C. J. Vineis, and G. W. Turner, Terahertz quantum-cascade-laser source based on intracavity difference-frequency generation, Nat. Photonics **1**, 288 (2007).
[13] K. Fujita, S. Jung, Y. Jiang, J. H. Kim, A. Nakanishi, A. Ito, M. Hitaka, T. Edamura, and M. A. Belkin, Recent progress in terahertz difference-frequency quantum cascade laser sources, Nanophotonics **7**, 1795 (2018).

[14] L. Ozyuzer, A. E. Koshelev, C. Kurter, N. Gopalsami, Q. Li, M. Tachiki, K. Kadowaki, T. Yamamoto, H. Minami, H. Yamaguchi, T. Tachiki, K. E. Gray, W.-K. Kwok, and U. Welp, Emission of coherent THz radiation from superconductors, Science **318**, 1291 (2007).

[15] R. Kleiner, F. Steinmeyer, G. Kunkel, and P. Müller, Intrinsic Josephson Effects in $Bi_2Sr_2CaCu_2O_8$ Single Crystals, Phys. Rev. Lett. **68**, 2394 (1992).

[16] B. D. Josephson, Possible new effects in superconductive tunneling, Phys. Lett. **1**, 251 (1962).

[17] U. Welp, K. Kadowaki, and R. Kleiner, Superconducting emitters of THz radiation, Nat. Photonics **7**, 702 (2013).

[18] M. Darula, T. Doderer, and S. Beuven, Millimetre and sub-mm wavelength radiation sources based on discrete Josephson junction arrays, Supercond. Sci. Technol. **12**, R1 (1999).

[19] H. B. Wang, S. Guénon, B. Gross, J. Yuan, Z. G. Jiang, Y. Y. Zhong, M. Grünzweig, A. Iishi, P. H. Wu, T. Hatano, D. Koelle, and R. Kleiner, Coherent Terahertz Emission of Intrinsic Josephson Junction Stacks in the Hot Spot Regime, Phys. Rev. Lett. **105**, 057002 (2010).

[20] R. A. Klemm and K. Kadowaki, Output from a Josephson stimulated terahertz amplified radiation emitter, J. Phys.: Condens. Matter **22**, 375701 (2010).

[21] H. Minami, C. Watanabe, K. Sato, S. Sekimoto, T. Yamamoto, T. Kashiwagi, R. A. Klemm, and K. Kadowaki, Local SiC photoluminescence evidence of hot spot formation and sub-THz coherent emission from a rectangular $Bi_2Sr_2CaCu_2O_{8+\delta}$ mesa, Phys. Rev. B **89**, 054503 (2014).

[22] C. Watanabe, H. Minami, T. Yamamoto, T. Kashiwagi, R. A. Klemm, and K. Kadowaki, Spectral investigation of hot spot and cavity resonance effects on the terahertz radiation from high-T_c superconducting $Bi_2Sr_2CaCu_2O_{8+\delta}$ mesas, J. Phys.: Condens. Matter **26**, 172201 (2014).

[23] T. Kashiwagi, T. Yamamoto, H. Minami, M. Tsujimoto, R. Yoshizaki, K. Delfanazari, T. Kitamura, C. Watanabe, K. Nakade, T. Yasui, K. Asanuma, Y. Saiwai, Y. Shibano, T. Enomoto, H. Kubo, K. Sakamoto, T. Katsuragawa, B. Marković, J. Mirković, R. A. Klemm, and K. Kadowaki, Efficient Fabrication of Intrinsic-Josephson-Junction Terahertz Oscillators with Greatly Reduced Self-Heating Effects, Phys. Rev. Appl. **4**, 054018 (2015).

[24] T. Kashiwagi, T. Yamamoto, T. Kitamura, K. Asanuma, C. Watanabe, K. Nakade, T. Yasui, Y. Saiwai, Y. Shibano, H. Kubo, K. Sakamoto, T. Katsuragawa, M. Tsujimoto, K. Delfanazari, R. Yoshizaki, H. Minami, R. A. Klemm, and K. Kadowaki, Generation of electromagnetic waves from 0.3 to 1.6 terahertz with a high-T_c superconducting $Bi_2Sr_2CaCu_2O_{8+\delta}$ intrinsic Josephson junction emitter, Appl. Phys. Lett. **106**, 092601 (2015).

[25] T. Kashiwagi, K. Sakamoto, H. Kubo, Y. Shibano, T. Enomoto, T. Kitamura, K. Asanuma, T. Yasui, C. Watanabe, K. Nakade, Y. Saiwai, T. Katsuragawa, M. Tsujimoto, R. Yoshizaki, T. Yamamoto, H. Minami, R. A. Klemm, and K. Kadowaki, A high-T_c intrinsic Josephson junction emitter tunable from 0.5 to 2.4 terahertz, Appl. Phys. Lett. **107**, 082601 (2015).

[26] E. A. Borodianskyi and V. M. Krasnov, Josephson emission with frequency span 1–11 THz from small $Bi_2Sr_2CaCu_2O_{8+\delta}$ mesa structures, Nat. Commun. **8**, 1742 (2017).

[27] S. Sekimoto, C. Watanabe, H. Minami, T. Yamamoto, T. Kashiwagi, R. A. Klemm, and K. Kadowaki, Continuous 30 μW terahertz source by a high-T_c superconductor mesa structure, Appl. Phys. Lett. **103**, 182601 (2013).

[28] I. Kakeya and H. B. Wang, Terahertz-wave emission from Bi2212 intrinsic Josephson junctions: A review on recent progress, Supercond. Sci. Technol. **29**, 073001 (2016).

[29] R. Kleiner and H. B. Wang, Terahertz emission from $Bi_2Sr_2CaCu_2O_{8+\delta}$ intrinsic Josephson junction stacks, J. Appl. Phys. **126**, 171101 (2019).

[30] T. M. Benseman, K. E. Gray, A. E. Koshelev, W.-K. Kwok, U. Welp, H. Minami, K. Kadowaki, and T. Yamamoto, Powerful terahertz emission from $Bi_2Sr_2CaCu_2O_{8+\delta}$ mesa arrays, Appl. Phys. Lett. **103**, 022602 (2013).

[31] G. Kuwano, M. Tsujimoto, Y. Kaneko, T. Imai, Y. Ono, S. Nakagawa, S. Kusunose, H. Minami, T. Kashiwagi, K. Kadowaki, Y. Simsek, U. Welp, and W.-K. Kwok, Mesa-Sidewall Effect on Coherent Terahertz Radiation via Spontaneous Synchronization of Intrinsic Josephson Junctions in $Bi_2Sr_2CaCu_2O_{8+\delta}$, Phys. Rev. Appl. **13**, 014035 (2020).

[32] K. Kadowaki, M. Tsujimoto, K. Yamaki, T. Yamamoto, T. Kashiwagi, H. Minami, M. Tachiki, and R. A. Klemm, Evidence for a dual-source mechanism of terahertz radiation from rectangular mesas of single crystalline $Bi_2Sr_2CaCu_2O_{8+\delta}$ intrinsic Josephson junctions, J. Phys. Soc. Jpn. **79**, 023703 (2010).

[33] H. Minami, I. Kakeya, H. Yamaguchi, T. Yamamoto, and K. Kadowaki, Characteristics of terahertz radiation emitted from the intrinsic Josephson junctions in high-T_c superconductor $Bi_2Sr_2CaCu_2O_{8+\delta}$, Appl. Phys. Lett. **95**, 232511 (2009).

[34] H. Minami, T. Koike, N. Orita, T. Kashiwagi, M. Tsujimoto, T. Yamamoto, and K. Kadowaki, Coupling to external structures : Boundary conditions for the Bi2212-based superconducting THz emitter, J. Phys.: Conf. Ser. **400**, 022072 (2012).

[35] H. Asai, M. Tachiki, and K. Kadowaki, Proposal of terahertz patch antenna fed by intrinsic Josephson junctions, Appl. Phys. Lett. **101**, 112602 (2012).

[36] R. A. Klemm, A. E. Davis, Q. X. Wang, T. Yamamoto, D. P. Cerkoney, C. Reid, M. L. Koopman, H. Minami, T. Kashiwagi, J. R. Rain, C. M. Doty, M. A. Sedlack, M. A. Morales, C. Watanabe, M. Tsujimoto, K. Delfanazari, and K. Kadowaki, Terahertz emission from the intrinsic Josephson junctions of high-symmetry thermally-managed $Bi_2Sr_2CaCu_2O_{8+\delta}$ microstrip antennas, IOP Conf. Ser.: Mater. Sci. Eng. **279**, 012017 (2017).

Correction: During the final production stage, a mistake was made in finalizing the author list for Ref. [23] and has been set right.